

Synthesis of gadolinium titanate based nanocrystalline multicomponent rare earth oxides

Anton V. Guskov, Pavel G. Gagarin, Vladimir N. Guskov, Konstantin S. Gavrichev

Kurnakov Institute General and Inorganic Chemistry Russian Academy of Sciences, Moscow, Russia

Corresponding author: V.N. Guskov, guskov@igic.ras.ru

ABSTRACT Optimal conditions for the synthesis of single-phase crystalline and nanocrystalline multicomponent oxides based on pyrochlore structure gadolinium titanate have been determined. The parameters of cubic lattices were determined and the morphology of the surface of RE titanates was studied.

KEYWORDS titanates, synthesis, nanocrystalline pyrochlore

ACKNOWLEDGEMENTS This study was carried out in the frameworks of research project “Solving the actual problems using charged particle beams of the NICA complex” (State assignment No. 1024050300012-6-1.4.2)

FOR CITATION Guskov A.V., Gagarin P.G., Guskov V.N., Gavrichev K.S. Synthesis of gadolinium titanate based nanocrystalline multicomponent rare earth oxides. *Nanosystems: Phys. Chem. Math.*, 2024, **15** (6), 774–780.

1. Introduction

Mixed oxides of composition $RE_2B_2O_7$ (RE=rare-earth elements, B=Ti, Zr, Hf) with pyrochlore structure type (*Fd3m*) are characterized by a high melting point and absence of structural phase transitions in a wide temperature range of existence, with the exception of disordering occurring at temperatures above 1800 °C and transformation into a phase of defective fluorite (*Fm3m*) [1–3]. High chemical and thermal stability of these substances, as well as low thermal conductivity, allows them to be considered as materials for thermal barrier coatings [4, 5], solid electrolytes for SOFC [6], as well as scintillators, phosphors and dielectrics [7, 8]. In addition, pyrochlores are recognized as the most promising materials for the immobilization of actinides in the nuclear fuel cycle due to their low solubility in acids and water and resistance to radiation exposure [9–11]. Actinides (3+) are able to replace the rare earth element in the RE position, while (4+) actinides can be placed in the B position. In any case, the internal decay of radionuclides leads to the transition of the matrix to an amorphous state as defects accumulate [12], which can lead to the actinides release. Radiation damage modeling and determination of maximum doses are carried out based on the results of irradiation with heavy ion beams [13]. These studies have demonstrated that the effects of radiation depend both on the ratio of the radii of $r(RE^{3+})/r(B^{4+})$ cations, since the probability of amorphization increases with its increase, and on the nature of cation B, since replacing Ti^{4+} with Zr^{4+} increases radiation resistance [14–16].

At the same time, zirconates of “heavy” lanthanides having the structure of defective fluorite, i.e. $Er_2O_3 \cdot 2ZrO_2$, retain their crystalline structure at higher doses of radiation and turn out to be more radiation-resistant materials than pyrochlores. (Here it should be noted that zirconates and hafnates of “heavy” lanthanides and yttrium are solid solutions with a wide homogeneity range based on cubic zirconium dioxide and should be represented as $(1-x)RE_2O_3 \cdot 2xZrO_2$, $x \sim 0.4 - 1.0$, and the writing $RE_2Zr_2O_7$ adopted in a number of articles for Ln=Tb–Lu and Y, i.e. $x = 0.5$, is in fact not correct [17].)

Modeling of defect formation under the action of ionizing radiation confirms the general concept of the relative stability of pyrochlores, but does not take into account such phenomena as dynamic annealing, migration and recombination of defects under the action of radiation, and also does not explain the influence of the size of the RE^{+3} cation and the type of crystal structure [14]. The influence of the degree of crystallinity of the material is also unknown. The studies carried out in [16] showed the existence of a critical amorphization temperature T_c , above which rapid recrystallization of radiation damage occurs, and amorphization of the sample is not proceed due to kinetic reasons. An important consequence of the work [16] results is that the critical temperature of amorphization increases with an increase in the mass of a heavy ion, creating a larger cascade of damage. Titanates of rare earth elements are convenient objects for studying the effects of heavy ion beams due to their cubic structure, relatively wide area of homogeneity and satisfactory response to radiation exposure [18]. In [14], a systematic determination of the amorphization temperature of a number of single-crystal lanthanide (Sm–Lu) and yttrium titanates of the pyrochlore structural type was performed under the action of a Kr^+ beam with an energy of 1 MeV. It was found that gadolinium titanate ($T_c = 1120$ K) has the highest amorphization temperature, which decreases both with an increase in the radius of the rare earth element to samarium titanate ($T_c = 1045$ K) and with a decrease in the radius of RE^{+3} during the transition from gadolinium to lutetium titanate ($T_c = 480$ K). A decrease in the critical temperature of amorphization means an increase in resistance to radiation damage. From this fact, it was concluded in [14] that pyrochlores, which are closer to the ideal structure of fluorite, are also more resistant to ion beam

amorphization. The authors [14] attribute the unusual behavior of T_c in a series of titanates not only to a change in RE^{3+} radius, but also to a change in the nature of the chemical bond, which, as stated, depends on the degree of filling of the 4f electron shell: in gadolinium, it is half filled, and in lutetium it is completely filled. Determination of the enthalpy of formation of lanthanide titanates and yttrium $RE_2Ti_2O_7$ [19] by the measuring of enthalpy of dissolution in oxide melt showed that with a decrease in the radius of the RE^{3+} ion, the enthalpy stability of titanates with respect to simple oxides decreases and correlates with the amorphization temperatures given in [14]. Recently, special attention has been paid to new materials based on multicomponent solid solutions of oxides for use in extreme conditions, including for the immobilization of radioactive waste, since the introduction of several various cations leads to defects of the crystal lattice that prevent the accumulation of damage in materials and stop the spread of 1-D defects [20]. An increase in the stability of such materials is achieved by reducing the Gibbs free energy owing to an increase in the configuration entropy due to an increase in the number of components of the solid solution. At the same time, varying the number and ratio of components allows you to control the functional properties of materials, limit grain growth, reduce thermal conductivity due to phonon scattering, and increase thermal and radiation stability. Traditionally, three- and four-component solid solutions are considered to be “middle entropy”, and five- and higher – “highentropy” [21]. In [22], the effect of a 3 MeV beam of Au^{2+} ions on medium- and multicomponent pyrochlores based on gadolinium titanate was studied and it was found that with an increase in the dose load, the structure of pyrochlore turns into defective fluorite, and then amorphization occurs, and high entropy pyrochlore $(GdDyHoErYb)_{2/5}Ti_2O_7$ showed the minimum tendency to amorphization. Authors concluded that the greatest influence on depreciation is exerted not by the entropy factor, but by the ratio of the radii of $r(RE^{3+})/r(B^{4+})$ cations. The effects of heavy ion beams on the nanocrystalline structures of simple and complex titanates remained outside the scope of the studies considered, although nanocrystalline substances are characterized by increased Gibbs energy, and, therefore, should have a reduced amorphization temperature T_c of relatively well-crystallized oxides, moreover, it is unknown whether irradiation will lead to amorphization of nanocrystalline matter or, conversely, to recrystallization, according to at least at the initial stage.

The goal of this study was to develop a method for the synthesis of “high-entropy titanates” for subsequent experiments to study amorphization under the action of a high-energy heavy ion beams conducted within the framework of the ARIADNA project: applied Research at the NICA complex.

2. Experimental

To carry out such research, it is necessary to determine the optimal method for the synthesis of nanocrystalline titanates. As is known, during the synthesis of lanthanide zirconates or hafnates by “reverse” deposition followed by annealing at a high temperature (800 – 1300 °C), a nanoscale fluorite-like phase is formed, and calcination at temperatures > 1500 °C is required for the complete interaction of the components and the formation of crystalline pyrochlores [17, 23, 24]. The method is convenient because it allows you to control the synthesis at all stages – from the synthesis of a hydroxide precursor of a given composition to the intermediate stages of heat treatment.

The $TiOSO_4 \cdot xH_2O$ (Sigma-Aldrich 99.99 wt.%), Gd_2O_3 (99.998 wt. %), Sm_2O_3 (99.998 wt. %), Dy_2O_3 (99.998 wt. %) and Tb_2O_3 (99.998 wt. %) LANHIT, Y_2O_3 (99.998 wt. %), hydrochloric acid (35 – 38 wt. % HCl, Os. Ch. qualification) and ammonia solution (25 – 28 wt. % NH_4OH) produced by KHIMMED were used as starting materials for the synthesis of gadolinium titanate-based samples. A simultaneous thermal analysis unit STA 449F1 Jupiter (NETZSCH-Gerätebaug GmbH) was used for thermal analysis using the DSC/TG method, and X-ray phase analysis was performed using a diffractometer D8 Advance (CuK α , $\lambda = 1.5418 \text{ \AA}$, Ni filter, LYNXEYE detector, reflection geometry) in the angle range $2\theta = 10^\circ - 80^\circ$. The morphology of the samples was studied using a TESCAN AMBER electron microscope with a Bright Beam non-immersion column and an ultra-high resolution of 1.3 nm at an accelerating voltage of 1 kV. The data [25] were used to calculate the molar masses of the samples, and average radii of the cations were estimated using the recommended in [26] values.

3. Results and discussion

Multicomponent oxides based on gadolinium titanate, samarium, terbium and dysprosium, as well as yttrium, were selected for the research (Table 1), in contrast to the work [22], where additional elements to gadolinium were Dy, Ho, Er, Yb and Nd. The choice of additional elements in this study, as in [22], is quite arbitrary, however, it must satisfy the condition $1.46 < r(RE^{3+})/r(B^{4+}) < 1.78$ for the implementation of the $Fd3m$ pyrochlore structure [1]. Low values (<1.46) are typical for the structural type of defective fluorite $Fm3m$, and higher values (>1.78) are typical for the monoclinic perovskite lattice $P21$.

To carry out the synthesis, titanyl sulfate was dissolved in water, and oxides of rare earths were dissolved in hydrochloric acid. The molal concentration of metals in solutions in terms of oxides were determined by the weight method, precipitating metal hydroxides with an aqueous solution of ammonia, followed by drying and calcination to a temperature of 1000 °C. The weight method of initial solutions mixing allows you to more accurately obtain the stoichiometric ratio of metals. (The use of molal concentrations, firstly, is due to the possibility of using more concentrated solutions due to the fact that the accuracy of weighing significantly exceeds the accuracy of determining volume, and, secondly,

TABLE 1. Composition of studied specimens, molar mass, middle ionic radius RE^{3+} (CN=8), ratio of cationic radii $(RE^{3+})/r(B^{4+})$, calculated and experimental unit cell parameters of pyrochlore structure (a) and maximum temperatures of transition in DSC curves

Composition	Molar mass, g-mol	Middle radius $r(RE^{3+})$, Å	$r(RE^{3+})/r(Ti^{4+})$	Lattice parameter a , Å		DSC t_{max} , °C
				Calc. from [27]	Experiment	
$Gd_2Ti_2O_7$	522.2298	1.053	1.74	10.1838(2)	10.185(1)	838
$GdSmTi_2O_7$	515.3398	1.066	1.76	10.2074	10.198(3)	824
$Gd_{2/3}Sm_{2/3}Y_{2/3}Ti_2O_7$	472.0737	1.050	1.74	10.1698	10.169(9)	813
$Gd_{1/2}Sm_{1/2}Y_{1/2}Dy_{1/2}Ti_2O_7$	487.23773	1.044	1.73	10.1607	10.162(7)	806
$Gd_{2/5}Sm_{2/5}Y_{2/5}Dy_{2/5}Tb_{2/5}Ti_2O_7$	494.90628	1.043	1.72	10.1588	10.159(1)	809

molal concentrations are temperature independent). The prepared solution was added dropwise with intensive stirring to a concentrated ammonia solution taken in excess. The sediment was washed, centrifuged and dried at 90 °C for 72 hours. Samples of the obtained substances were studied by DSC/TG analysis to determine the temperature stages of formation of crystalline pyrochlores from pre-dried hydroxides, Fig. 1.

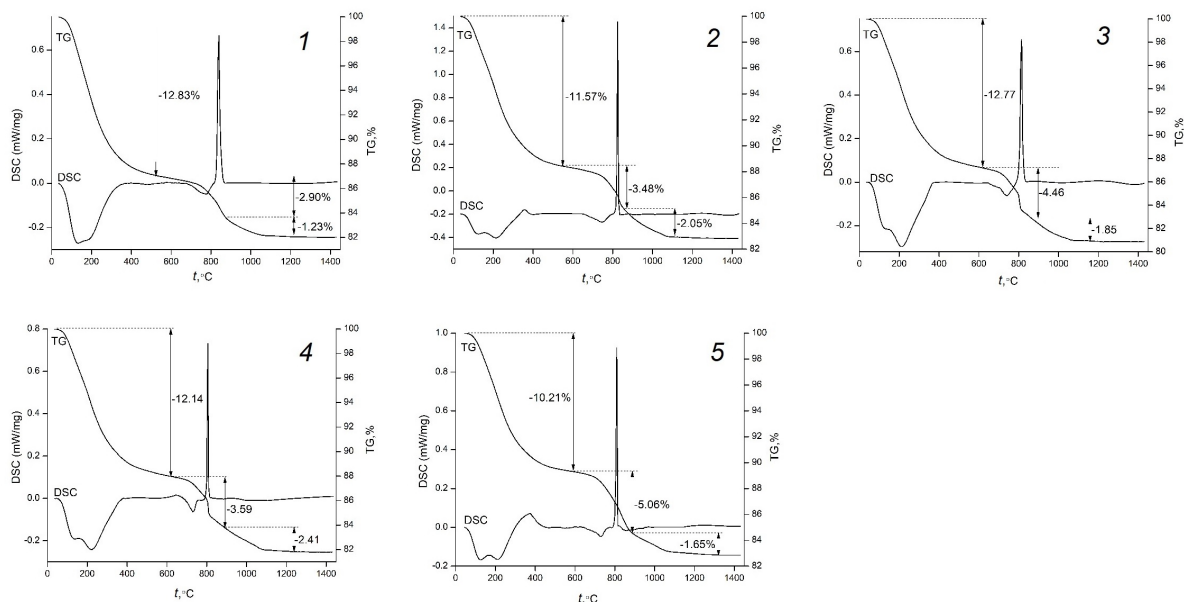


FIG. 1. DSC/TG curves of dried hydroxide precursors: 1) $Gd_2Ti_2O_7$, 2) $GdSmTi_2O_7$, 3) $Gd_{2/3}Sm_{2/3}Y_{2/3}Ti_2O_7$, 4) $Gd_{1/2}Sm_{1/2}Y_{1/2}Dy_{1/2}Ti_2O_7$, 5) $Gd_{2/5}Sm_{2/5}Y_{2/5}Dy_{2/5}Tb_{2/5}Ti_2O_7$

The common view of the DSC/TG heating curves (Fig. 1) for all 5 samples is similar and can be subdivided into 3 stages: at the first stage of heating (75 – 500 °C), an endothermic effect is observed, which is accompanied by a loss of mass corresponding to $\sim 2.5 - 3$ water molecules per mole of the substance. Further heating (the second stage) from 500 to 900 °C is accompanied by dehydroxylation with a loss of $\sim 1.5 - 2$ H_2O , while in the region of 800 – 850 °C there is a sharp exothermic effect corresponding to the formation of hydroxylated pyrochlore of the probable composition $RE_2Ti_2O_6 \cdot 5OH$, and the temperature of the maximum t_{max} of transformation decreases slightly with an increase in the number of RE-elements (Table 1). The residual hydroxyl group is revealed only at the third stage in the range of $\sim 900 - 1000$ °C to form compounds of the structural type of pyrochlore $RE_2Ti_2O_7$. Unlike the $RE_2O_3-ZrO_2$ and $RE_2O_3-HfO_2$ systems, in which, with this synthesis method and these temperatures, a nanoscale metastable phase of the structural type of disordered fluorite is formed [17, 23, 24], in the $Gd_2O_3-TiO_2$ system, a fluorite-like phase is not found either in a stable or metastable state [28]. To determine the sequence of processes occurring during the heating of precursors, samples of dried precursors were calcinated for 2 hours at 700, 1000 and 1500 °C, and were studied by X-ray diffraction phase analysis. Fig. 2 shows XRD patterns of the annealed $Gd_2Ti_2O_7$ sample. As can be seen, at 700 °C (curve 1), a pattern typical for the amorphous state of the sample is observed. Calcination of the samples above the component interaction temperature (1000 °C, curve 2) leads to the formation of a sample of the structural type of pyrochlore, as evidenced by

the characteristic diffraction reflections 111, 311, 331 and 511. At the same time, the size of the crystallites (according to the results of the Debye–Scherrer evaluation) is about 35 nm, which corresponds to the range of nanoscales (< 100 nm). And finally, annealing at 1500 °C (curve 3) leads to a significant change in diffractograms, associated with the formation of narrower and more pronounced reflexes, which indicates satisfactory crystallization of the sample and on the size of the crystallites beyond the nanoscale region.

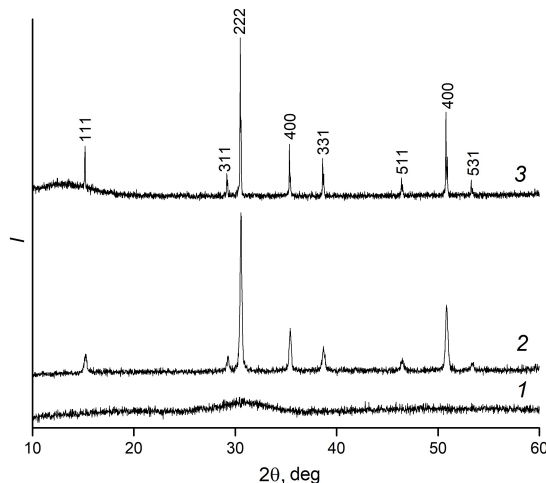


FIG. 2. XRD patterns of $Gd_2Ti_2O_7$ precursor annealed at 1 – 700 °C, 2 – 1000 °C, 3 – 1500 °C

Diffraction studies performed for all samples of solid solutions of RE titanates prepared at a temperature of 1000 °C are shown in Fig. 3. They confirm the formation of single-phase crystalline compounds of the pyrochlore structural type. It must be noted that in the case of multicomponent compounds and solid solutions, it is not possible to use the Debye–Scherrer approximation to estimate the size of coherent scattering regions due to distortions of the crystal lattice leading to broadening of diffraction reflections. A comparison of these results with the diffractograms shown in Fig. 4 of samples well crystallized by annealing at 1500 °C indicates a possible nanoscale particle size of specimens obtained at 1000 °C. It is possible to confirm the size of synthesized samples by conducting scanning electron microscopy (SEM) studies. Scanning microscopy of the surface of powdered samples annealed at 1000 °C (Fig. 5), even with the maximum magnification available for these substances of 80,000× does not allow to assess the size of the crystallites due to the nanoscale state of the samples, whereas after annealing at a temperature of 1500 °C, larger particles (> 100 nm) form a monolithic (and, probably, gas-tight) surface structure (Fig. 6).

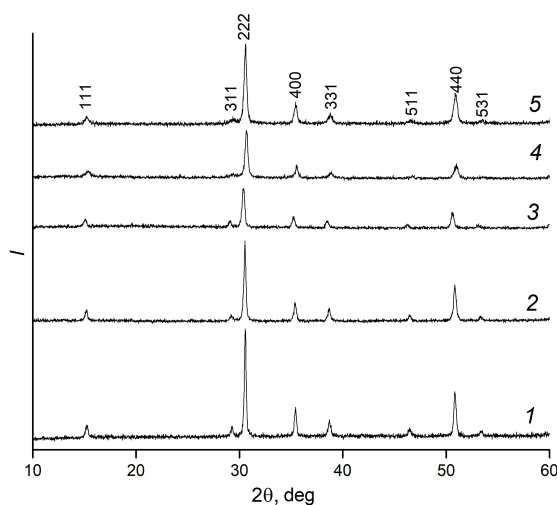


FIG. 3. XRD patterns for annealed at 1000 °C RE titanates: 1) $Gd_2Ti_2O_7$, 2) $GdSmTi_2O_7$, 3) $Gd_{2/3}Sm_{2/3}Y_{2/3}Ti_2O_7$, 4) $Gd_{1/2}Sm_{1/2}Y_{1/2}Dy_{1/2}Ti_2O_7$, 5) $Gd_{2/5}Sm_{2/5}Y_{2/5}Dy_{2/5}Tb_{2/5}Ti_2O_7$

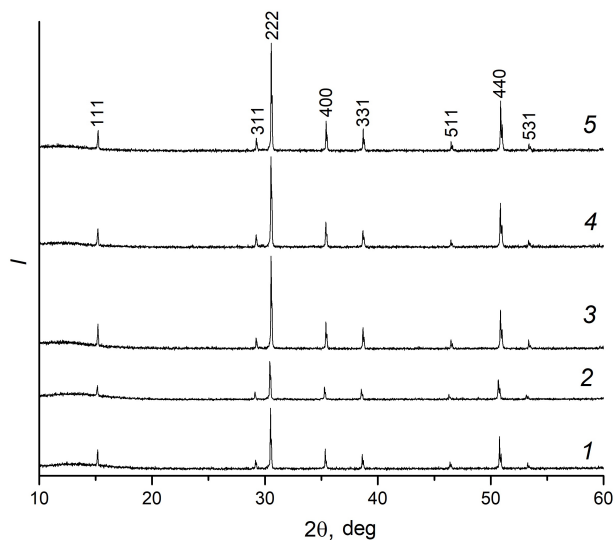


FIG. 4. XRD patterns of RE titanates annealed at 1500 °C: 1) $Gd_2Ti_2O_7$, 2) $GdSmTi_2O_7$, 3) $Gd_{2/3}Sm_{2/3}Y_{2/3}Ti_2O_7$, 4) $Gd_{1/2}Sm_{1/2}Y_{1/2}Dy_{1/2}Ti_2O_7$, 5) $Gd_{2/5}Sm_{2/5}Y_{2/5}Dy_{2/5}Tb_{2/5}Ti_2O_7$

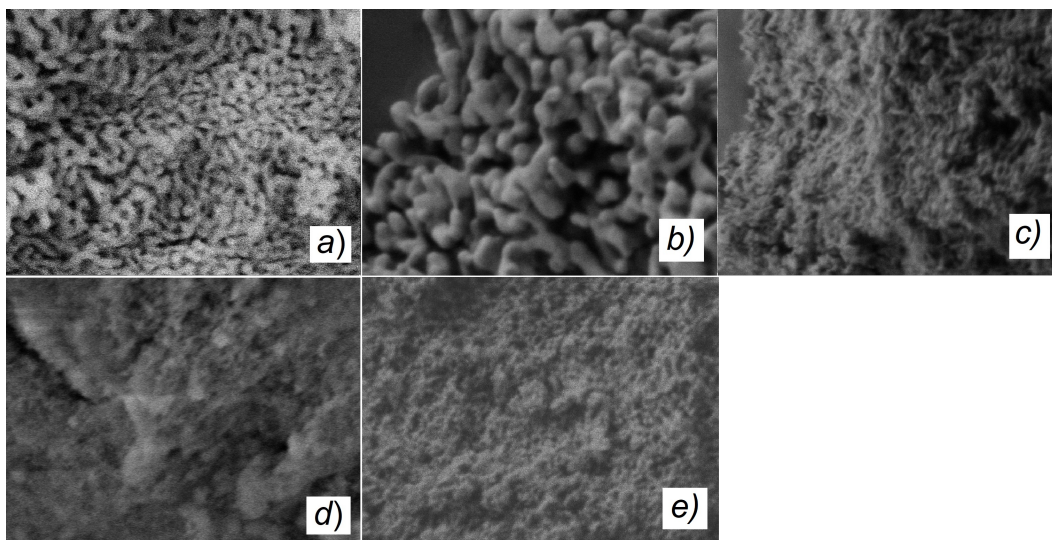


FIG. 5. Surface morphology of specimens annealed at 1000 °C: a) $Gd_2Ti_2O_7$, b) $GdSmTi_2O_7$, c) $Gd_{2/3}Sm_{2/3}Y_{2/3}Ti_2O_7$, d) $Gd_{1/2}Sm_{1/2}Y_{1/2}Dy_{1/2}Ti_2O_7$, e) $Gd_{2/5}Sm_{2/5}Y_{2/5}Dy_{2/5}Tb_{2/5}Ti_2O_7$, $\times 80\ 000$

4. Conclusions

The sequence of phase transformations during the formation of nanoscale gadolinium titanate based multicomponent oxides of rare earth elements with a pyrochlore structure was determined as a result of the conducted investigations. The temperature ranges of separate stages of process of their formation were determined.

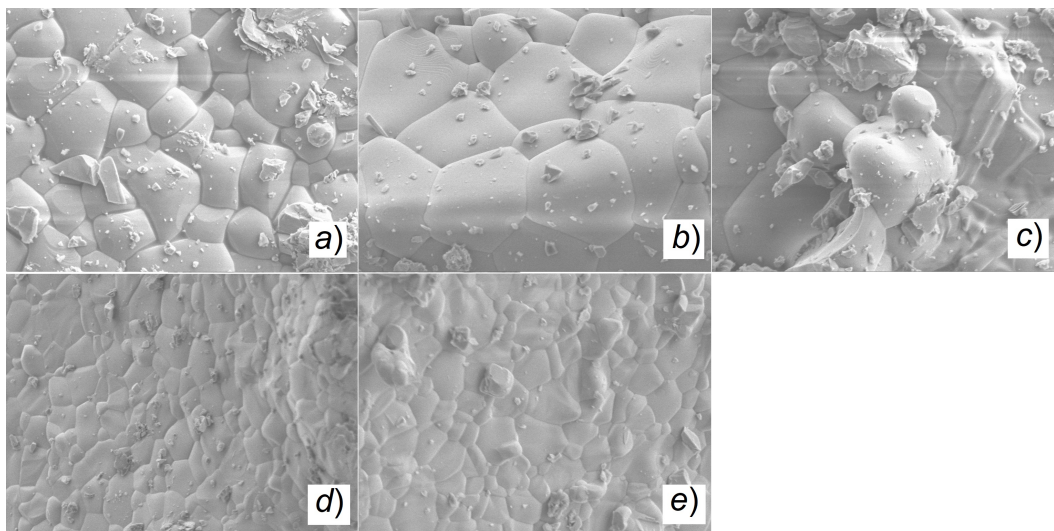


FIG. 6. Surface morphology of specimens annealed at 1500 °C: a) $\text{Gd}_2\text{Ti}_2\text{O}_7$, b) $\text{GdSmTi}_2\text{O}_7$, c) $\text{Gd}_{1/3}\text{Sm}_{2/3}\text{Y}_{2/3}\text{Ti}_2\text{O}_7$, d) $\text{Gd}_{1/2}\text{Sm}_{1/2}\text{Y}_{1/2}\text{Dy}_{1/2}\text{Ti}_2\text{O}_7$, e) $\text{Gd}_{2/5}\text{Sm}_{2/5}\text{Y}_{2/5}\text{Dy}_{2/5}\text{Tb}_{2/5}\text{Ti}_2\text{O}_7$, $\times 30\,000$

References

- [1] Andrievskaya E.R. Phase equilibria in the refractory oxide systems of zirconia, hafnia and yttria with rare-earth oxides. *J. Europ. Ceram. Soc.*, 2008, **28**, P. 2363–2388.
- [2] Komissarova L.N., Shatsky V.M., Pushkina G.Ya., Scherbakova L.G., Mamsurova L.G., Sukhanova G.E. *Rare-earth compounds. Carbonates, oxalates, nitrates, titanates*. Nauka Publ. Co. 1984. 235 p.
- [3] Subramanian M.A., Aravamudan G., Subba Rao G.V. Oxide pyrochlores—A review. *Prog. Solid State Chem.*, 1983, **15**, P. 55–143.
- [4] Clarke D. R., Phillpot S. R. Thermal barrier coating materials. *Materials Today*, 2005, **8**, P. 22–29.
- [5] Vaßen R., Jarligo M.O., Steinke T., Mack D.E., Stöver D. Overview on advanced thermal barrier coatings. *Surf. Coat. Techn.*, 2010, **205**, P. 938–942.
- [6] Yamamura H. Electrical conductivity anomaly around fluorite-pyrochlore phase boundary. *Solid State Ionics*, 2003, **158**, P. 359–365.
- [7] Brixner L.H. Structural and luminescent properties of the $\text{Ln}_2\text{Hf}_2\text{O}_7$ -type rare earth hafnates. *Mater. Res. Bull.*, 1984, **19**, P. 143–149.
- [8] Ji Y., Jiang D., Shi J. $\text{La}_2\text{Hf}_2\text{O}_7:\text{Ti}^{4+}$ ceramic scintillator for X-ray imaging. *J. Mater. Res.*, 2005, **20**, P. 567–570.
- [9] Ewing R.C., Weber W.J., Lian J. Nuclear waste disposal pyrochlore ($\text{A}_2\text{B}_2\text{O}_7$): nuclear waste form for the immobilization of plutonium and “minor” actinides. *J. Appl. Phys.*, 2004, **95**, P. 5949–5971.
- [10] McMaster S.A., Ram R., Faris N., Powenby M.I. Radionuclide disposal using the pyrochlore supergroup of minerals as a host matrix. A review. *J. Hazard Mater.*, 2018, **360**, P. 257–269.
- [11] Wang Y., Jing C., Ding Z.Y., Zhang Y.Z., Wei T., Quang J.H., Liu Z.G., Wang Y.-J., Wang Y.-M. The structure, property, and ion irradiation effects of pyrochlores: a comprehensive review. *Crystals*, 2003, **13**.
- [12] Weber W.J., Ewing R.C., Plutonium immobilization and radiation effects. *Science*, 2000, **289** (5787), P. 2051–2052.
- [13] Lu X., Shu X., Wang L., Shao D., Zhang H., Zhang K., Xie Y. Heavy-ion irradiation effects on $\text{Gd}_2\text{Zr}_2\text{O}_7$ ceramics bearing complex nuclear waste. *J. Alloys Compd.*, 2019, **771**, P. 973–979.
- [14] Lian J., Chen J., Wang L.M., Ewing R.C. Radiation-induced amorphization of rare-earth titanate pyrochlores. *Phys. Rev. B*, 2003, **68**, 134107.
- [15] Sickafu K.E., Minervini I., Grimes R.W., Valdez J.A., Ishimaru M., Li F., McClellan K.J. Radiation tolerance of complex oxides. *Science*, 2000, **289** (5480), P. 748–751.
- [16] Wang S.X., Wang L.M., Ewing R.C., Govindan Kutti K.V. Ion irradiation effects for two pyrochlore compositions: $\text{Gd}_2\text{Ti}_2\text{O}_7$ and $\text{Gd}_2\text{Zr}_2\text{O}_7$. *Mat. Res. Soc. Symp. Proc.*, 1998, **540**, P. 355–360.
- [17] Guskov V.N., Gavrichev K.S., Gagarin P.G., Guskov A.V. Thermodynamic function of complex zirconia based lanthanide oxides-pyrochlores $\text{Ln}_2\text{Zr}_2\text{O}_7$ ($\text{Ln}=\text{La, Pr, Sm, Eu, Gd}$) and fluorites $\text{Ln}_2\text{O}_3 \cdot 2\text{ZrO}_2$ ($\text{Ln}=\text{Tb, Ho, Er, Tm}$). *Russ. J. Inorg. Chem.*, 2019, **64**, P. 1265–1281.
- [18] Yang D.Y., Xu C.P., Fu C.G., Zhang K.Q., Wang Y.Q., Li Y.H. Structure and radiation effect of Er-stuffed pyrochlore $\text{Er}_2(\text{Ti}_{2-x}\text{Er}_x)\text{O}_{7-x/2}$ ($x = 0 - 0.667$). *Nucl. Instr. Meth. Phys. Res. B*, 2015, **356–357**, P. 69–74.
- [19] Helean K.B., Ushakov S.V., Brown C.E., Navrotsky A., Lian J., Ewing R.C., Farmer J.M., Boatner L.A. Formation enthalpies of rare earth titanate pyrochlores. *J. Sol. State Chem.*, 2004, **177**, P. 1858–1866.
- [20] Ward T.Z., Wilkerson R.P., Muziko B.L., Foley A., Brahleg M., Weber W.J., Sickafus K.E., Mazza A.R. High entropy ceramics for applications in extreme environments. *J. Phys.: Mater.*, 2024, **7**, 021001.
- [21] Yeh J.W., Chen S.K., Lin S.J., Gan J.Y., Chin T.S., Shun T.T., Tsau C.H. Nanostructured high-entropy alloys with multiple principle: novel alloy design concepts and outcomes. *Advance Eng. Mater.*, 2004, **6**, P. 299–303.
- [22] Guo H., Zhang K., Li Y. Heavy-ion irradiation effects of high-entropy $\text{A}_2\text{Ti}_2\text{O}_7$ pyrochlore with multi-elements at site. *Ceram. Int.*, 2024, **50**, P. 21859–21868.
- [23] Gagarin P.G., Tyurin A.V., Guskov V.N., Khoroshilov A.V., Nikiforova G.E., Gavrichev K.S. Thermodynamic properties of p- $\text{Sm}_2\text{Zr}_2\text{O}_7$. *Inorgan. Mater.*, 2017, **53**, P. 619–625.
- [24] Guskov A.V., Gagarin P.G., Guskov V.N., Khoroshilov A.V., Gavrichev K.S. Thermal properties of solid solutions $\text{Ln}_2\text{O}_3 \cdot 2\text{HfO}_2$ ($\text{Ln} = \text{Dy, Ho, Er, Tm, Yb, Lu}$) at 300 – 1300 K. *Ceram. Int.*, 2021, **47**, P. 28004–28007.
- [25] Prohaska T., Irrgeher J., Benefield J., Böhlke J.K., Chesson L.A., Coplen T.B., Ding T., Dunn P. J.H., Gröning M., Holden N.E., Meijer H. A. J., Moossen H., Possolo A., Takahashi Y., Vogl J., Walczyk T., Wang J., Wieser M.E., Yoneda S., Zhu X.-K., Meija J. Standard atomic weights of the elements 2021 (IUPAC Technical Report). *Pure and Applied Chemistry*, 2022, **94**, P. 573–600.

- [26] Shannon R.D. Revised effective ionic radii and systematic studies of interatomic distances in halides and chalcogenides. *Acta Crystallogr. Sect. A: Cryst. Phys. Diffr. Theor. Gen. Crystallogr.*, 1976, **32**, P. 751–767.
- [27] ICDD PDF Database, <https://www.icdd.com/>
- [28] Waring J.L., Schneider S.J. Phase equilibrium relationships in the system Gd_2O_3 – TiO_2 . *J. Res. Nat. Bur. Stand. A*, 1965, **69**, P. 255–261.

Submitted 30 July 2024; revised 13 October 2024; accepted 16 October 2024

Information about the authors:

Anton V. Guskov – Kurnakov Institute General and Inorganic Chemistry Russian Academy of Sciences, 119991, Leninsky pr. 31, Moscow, Russia; ORCID 0000-0003-00826-5495; a.gus@igic.ras.ru

Pavel G. Gagarin – Kurnakov Institute General and Inorganic Chemistry Russian Academy of Sciences, 119991, Leninsky pr. 31, Moscow, Russia; ORCID 0000-0001-6450-3959; gagarin@igic.ras.ru

Vladimir N. Guskov – Kurnakov Institute General and Inorganic Chemistry Russian Academy of Sciences, 119991, Leninsky pr. 31, Moscow, Russia; ORCID 0000-0003-0425-8618; guskov@igic.ras.ru

Konstantin S. Gavrichev – Kurnakov Institute General and Inorganic Chemistry Russian Academy of Sciences, 119991, Leninsky pr. 31, Moscow, Russia; ORCID 0000-0001-5304-3555; gavrich@igic.ras.ru

Conflict of interest: the authors declare no conflict of interest.